Automatic Segmentation of the Pulmonary Lobes from Chest CT Scans Based on Fissures, Vessels, and Bronchi

Bianca Lassen, Eva M. van Rikxoort, Michael Schmidt, Sjoerd Kerkstra, Bram van Ginneken, and Jan-Martin Kuhnigk

***Abstract*—Segmentation of the pulmonary lobes is relevant in clinical practice and particularly challenging for cases with severe diseases or incomplete fissures. In this work an automated segmentation approach is presented that performs a marker-based watershed transformation on CT scans to subdivide the lungs into lobes. A cost image for the watershed transformation is computed by combining information from fissures, bronchi, and pulmonary vessels. The lobar markers are calculated by an analysis of the automatically labeled bronchial tree. By integration of information from several anatomical structures the segmentation is made robust against incomplete fissures.**

For evaluation the method was compared to a recently published method on 20 CT scans with no or mild disease. The average distances to the reference segmentation were 0.69 mm, 0.67 mm, and 1.21 mm for the left major, right major, and right minor fissure, respectively. In addition the results were submitted to LOLA11, an international lung lobe segmentation challenge with publically available data including cases with severe diseases. The average distances to the reference for the 55 CT scans provided by LOLA11 were 0.98 mm, 3.97 mm, and 3.09 mm for the left major, right major, and right minor fissure. Moreover, an analysis of the relation between segmentation quality and fissure completeness showed that the method is robust against incomplete fissures.

***Index Terms*—lung lobe segmentation, fissure segmentation**

I. Introduction

The human lungs are subdivided into five lobes that are separated by visceral pleura called pulmonary fissure. There are three lobes in the right lung, namely upper, middle, and lower lobe. The right upper and right middle lobe are divided by the right minor fissure whereas the right major fissure delimits the lower lobe from the rest of the lung. In the left lung there are only two lobes, the upper and the lower lobe, that are divided by the left major fissure (see Figure 1a). A characteristic of the pulmonary lobes are separated supply branches for both vessels and airways (see Figure 1b).

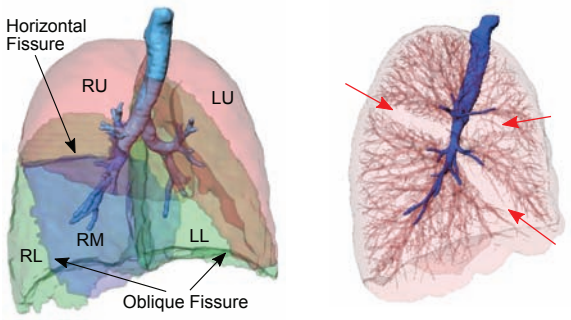

(a) Lung lobes. (b) Vessel and bronchi tree.

Fig. 1: Renderings of the anatomy of the lungs. a) shows a rendering of the lungs subdivided into the right upper (RU), right middle (RM), right lower (RL), left upper (LU), and left lower (LL) lobe. b) shows a rendering of the vessels (red) and bronchi (blue) tree of the right lung. There are no major supply branches at the lobar boundaries (arrows).

Lung lobe segmentation is relevant in clinical applications particularly for treatment planning. The location and distribution of pulmonary diseases are important parameters for the selection of a suitable treatment. Locally distributed emphysema can be treated more effective by lobar volume resection than homogeneously distributed emphysema [1]. Another application is quantitative monitoring of pulmonary diseases such as emphysema or fibrosis. A lobe-wise analysis shows the progression of the disease in more detail.

Computed tomography (CT) allows visualization of the lungs within a few seconds. Since typical scans with high anatomical details contain over 400 slices with submillimeter resolution for each direction, manual segmentation is time consuming and there is demand for automatic lung lobe segmentation methods.

The segmentation of pulmonary lobes is challenging because of anatomical variation and incomplete fissures. On the one hand, pathologies can deform the lobes and make the fissures unrecognizable. And on the other hand, even in patients with normal lung parenchyma the fissures are often not complete [2]. Examples of incomplete and deformed fissures are shown in Figure 2. For cases with incomplete fissures

B. Lassen is with Fraunhofer MEVIS, Bremen, Germany. E-mail: bianca.lassen@mevis.fraunhofer.de

E. M. van Rikxoort is with the Diagnostic Image Analysis Group, Department of Radiology, Radboud University Nijmegen Medical Centre, Nijmegen, The Netherlands and with Fraunhofer MEVIS, Bremen, Germany.

M. Schmidt is with Fraunhofer MEVIS, Bremen, Germany.

S. Kerkstra is with the Diagnostic Image Analysis Group, Department of Radiology, Radboud University Nijmegen Medical Centre, Nijmegen, The Netherlands.

B. van Ginneken is with the Diagnostic Image Analysis Group, Department of Radiology, Radboud University Nijmegen Medical Centre, Nijmegen, The Netherlands.

J.-M. Kuhnigk is with Fraunhofer MEVIS, Bremen, Germany.

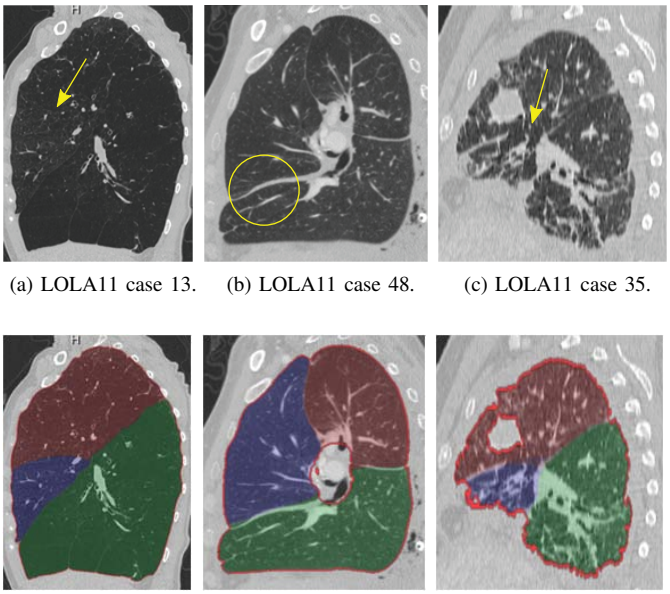

(a) LOLA11 case 13. (b) LOLA11 case 48. (c) LOLA11 case 35.

(d) LOLA11 case 13. (e) LOLA11 case 48. (f) LOLA11 case 35.

Fig. 2: Anatomical variation of pulmonary lobes. Figure a), b), and c) show a sagittal slice of the right lung. d), e), and f) show the same slices with labeled lobes (red = upper lobe, blue = middle lobe, green = lower lobe). a) shows a case with a small middle lobe and incomplete fissures (arrow). b) shows a case with a large middle lobe and pathologically thick fissures (circle). c) shows a pathological lung with several bright structures and incomplete fissures (arrow). Datasets are taken from LOLA11 [3].

radiologists infer the lobar boundaries using information from the bronchi and vessel trees. Since there are usually no major supply branches between the lung lobes (see Figure 1b) the lobar boundaries are defined in between the bronchi and vessel branches.

There are several different approaches of lung lobe and pulmonary fissure segmentation in literature. Van Rikxoort et al. [4], Wiemker et al. [5], Wang et al. [6], Pu et al. [7], and Wei et al. [8] presented methods for lobar fissure segmentation in CT data. For patients with complete pulmonary fissures a segmentation of these fissures is sufficient to obtain a lung lobe segmentation. Since in many cases fissures are incomplete additional processing steps are required to obtain a lobe segmentation. Nevertheless, the segmentation of visible fissures offers a good basis for lobe segmentation and can also be used for other purposes with clinical relevance such as quantifying the completeness of the fissures, which is an important feature for treatment planning of patients with emphysema [9].

Van Rikxoort et al. published two different lung lobe segmentation methods. In [10] pulmonary lobes and segments were found by supervised classification. First, the fissures were enhanced and segmented by the eigenvalues and eigenvectors of the Hessian matrix. Next, features such as the position relative to the fissures provided a labeling to a pulmonary lobe for every voxel inside the lung. The classifier was trained on 500 CT scans with findings that were assigned to a segment by an expert. The evaluation was done on 100 datasets with classified findings. For the left lung, 97% of the findings and for the right lung, 90% of the findings were assigned to the correct lobe. It did not produce anatomically correct results for cases with incomplete fissures.

The second lobe segmentation method by van Rikxoort et al. [11] is an automatic multi-atlas approach. First, the lungs, fissures, and bronchi were segmented automatically and combined into one cost image. A fast registration of this result with a set of five atlases with complete fissures gave the best matching atlas that was chosen for a fine registration to get the lobe segmentation result. The evaluation was done on two datasets. For 20 normal dose CT scans the mean distance to a manual fissure segmentation was 0.48 mm, 1.23 mm, and 1.28 mm for the left major, right major, and right minor fissure. The robustness of the segmentation against incomplete fissures was evaluated with an observer study on 100 low dose CT scans. Atlas-based methods are generally time-consuming, segmentation of one case took two hours on average. Another disadvantage of this approach was that scans with lobar shapes not represented in the atlas set were unlikely to be segmented correctly.

Kuhnigk et al. [12] presented a framework for automatic lung and lung lobe segmentation. The lobe segmentation was based on a watershed transformation that takes an analysis of lobar airways and vasculature into account. It was robust against missing fissures but therefore frequently inaccurate at clearly visible fissures. The method had been applied to more than 1000 datasets [13] but was not quantitatively validated.

Ukil and Reinhardt [14] presented a pulmonary lobe segmentation similar to Kuhnigk et al. [12]. In the first step, the lobes were segmented by a watershed transformation based on a distance map of the vasculature and markers from the labeled bronchi tree. In the second step, a 3D optimal surface detection was performed in a ROI around the initial segmented fissures to refine the lobe boundaries. As a last step, incomplete fissures were extrapolated based on a fast-marching method. The evaluation was done against a manual reference standard of the visible fissures from 12 cases with normal lungs and 17 cases with mild to moderate emphysema and showed a mean root-mean-square (rms) error of less than 2.7 mm over all fissures of all cases. A disadvantage of the method was that around 20-25% of the cases needed manual intervention.

Zhang et al. [15] created an anatomic atlas of the lungs that described the average position and variation of the major fissures from 16 CT datasets. The atlas was used for initialization of the fissures. A ridgeness operator enhanced the edges in the original images which offered information to refine the initial lobar boundaries. For the segmentation of the right minor fissure, the observer had to interactively set anchor points. The results were compared against manual tracings on 22 CT scans with normal anatomy and showed an average rms error of 1.96 ± 0.71 mm over all datasets. The approach was not evaluated on cases with abnormal anatomy or severe parenchymal diseases.

Pu et al. [16] proposed an automatic lobe segmentation method that started by detecting plane patches in subvolumes in the lungs. From these patches the pulmonary fissures were

inter- and extrapolated using implicit Radial Basis Functions. Based on the implicit functions representing the fissures, the lungs were divided into five lobes. No anatomical information of bronchi or vessels were taken into account in cases of incomplete fissures. A qualitative evaluation was done by visual inspection of two radiologist on 65 CT examinations of healthy or mildly diseased lungs. The evaluation showed that 50.8% of the cases were rated as "excellent" or "good" by both radiologists. The method was not evaluated on cases with severe lung diseases. Segmentation took on average 25 minutes for one case with a slice thickness of 0.625-1.25 mm.

Mori et al. [17] presented a lobe segmentation approach based on figure decomposition. First, the pulmonary fissures detected by an analysis of the Hessian matrix were subtracted from the lung ROI. Next, the lungs were eroded until there were two (in the left lung) respectively three (in the right lung) connected components left over. Labels were assigned to the components and the gaps were closed by dilation. Evaluation was performed on 13 CT datasets against a manually traced reference. The average coincident rates on the volume overlap were between 0.94 and 0.99 for the five lobes. The approach was not evaluated on lungs with severe diseases and it did not work for cases with missing fissures.

Ross et al. [18] published an interactive lobe segmentation method. An observer clicked on several parts of the fissures to create points that were extrapolated to complete fissures based on a thin plate spline interpolation method. Two observers applied the method to 20 CT scans and the distances of the results were compared. The average Euclidean distance of the user agreement was between 2.08 mm and 4.52 mm for the three fissures. An addition to this method was presented by Ross et al. [19] that was also based on a thin plate spline surface fitting but had no need for user interaction. Here, fissure particles were automatically detected by analysis of the eigenvalues and eigenvectors of the Hessian matrix and MAP estimation. This approach was evaluated on six CT scans and compared to two references created with the interactive version of this method [18]. The average distance to the references was between 1.78 mm and 2.95 mm for the three fissures. A drawback of this method was that it did not work for cases with missing fissures.

Lassen et al. [20] presented an interactive approach for lung lobe segmentation and correction of a given segmentation. An observer sketched the pulmonary fissure on slices of arbitrary orientation and got instant feedback in the form of an inter- and extrapolated fissure surface that covered the total lung. The interactive segmentation method was evaluated on the left fissures of 25 CT datasets against a manual segmentation by a human observer and showed an average distance of 1.57 ± 0.3 mm.

This paper proposes an automatic lung lobe segmentation method that uses information from automatic segmentations of the bronchi, vessels, and visible fissures in a 3D watershed transformation to be both robust against missing fissures and accurate at visible fissures. Although all previously published lobe segmentation methods described above were evaluated, it is not possible to compare the results directly because evaluation was performed on different datasets and with different evaluation measures (volume overlap, distance to the fissures, visual inspection).

In this paper, a direct comparison to two of the previously published methods is made: the atlas-based method by van Rikxoort et al. [11] and the method by Kuhnigk et al. [12]. For the direct comparison a set of 20 chest CT scans used in the original paper by van Rikxoort et al. [11] is used. To allow comparison to any lobe segmentation method, the proposed method was applied to a publicly available database from an international challenge for lung and lobe segmentation called LOLA11 [3]. LOLA11 provides 55 CT scans from different hospitals and scanners including lungs with severe pathologies. Participants can download the data and will get evaluation results after uploading the segmentation results. Submitted segmentation results are compared against a manual lobar border segmentation from a radiologist. Within the scope of LOLA11 a fair comparison of segmentation approaches is possible since all methods are evaluated on the same dataset with the same evaluation measures. The challenge is still open and offers an excellent opportunity to compare segmentation quality. Next to the evaluation measures provided by the LOLA11 challenge, we analyzed the segmentation accuracy in respect of the fissure completeness for the 55 cases of LOLA11.

II. Method

A lobe segmentation method is developed which combines anatomical information from the lungs, vessels, airways, and lobar fissures to obtain the lobes using a watershed-based segmentation method. The approach is an extension of the framework of Kuhnigk et al. [12] which performs a watershed-based lobe segmentation that does not make use of the lobar fissures and airways for construction of the cost image for the watershed segmentation. A preliminary version of the here presented approach without an extensive evaluation was previously published in [21] and [22].

Figure 3 provides an overview of the segmentation process. The method starts by segmenting the lungs, vessels, airways, and fissures, which are later combined into one cost image for the watershed segmentation process (Section II-B). In the first step lungs are segmented since all other segmentations are only performed inside the lung regions. A good lung segmentation is a prerequisite for the here presented lobe segmentation approach. The lung segmentation applied achieved the best performance in the LOLA11 [3] challenge. It is based on previous work [22] and therefore not described in this paper. Sections II-A1, II-A2, and II-A3 describe the segmentation of the vessels, fissures, and bronchi. Note that any vessel, airway, or fissure segmentation could be plugged into the method without adaptation.

A. Prerequisite segmentations

1) Pulmonary vessels: Based on the assumption that there are usually no major vessels at the lobar boundaries, the distance to the pulmonary vasculature is a suitable feature to detect lobar boundaries. To quantify the absence of vessels at the lobar boundaries, a coarse segmentation of the pulmonary

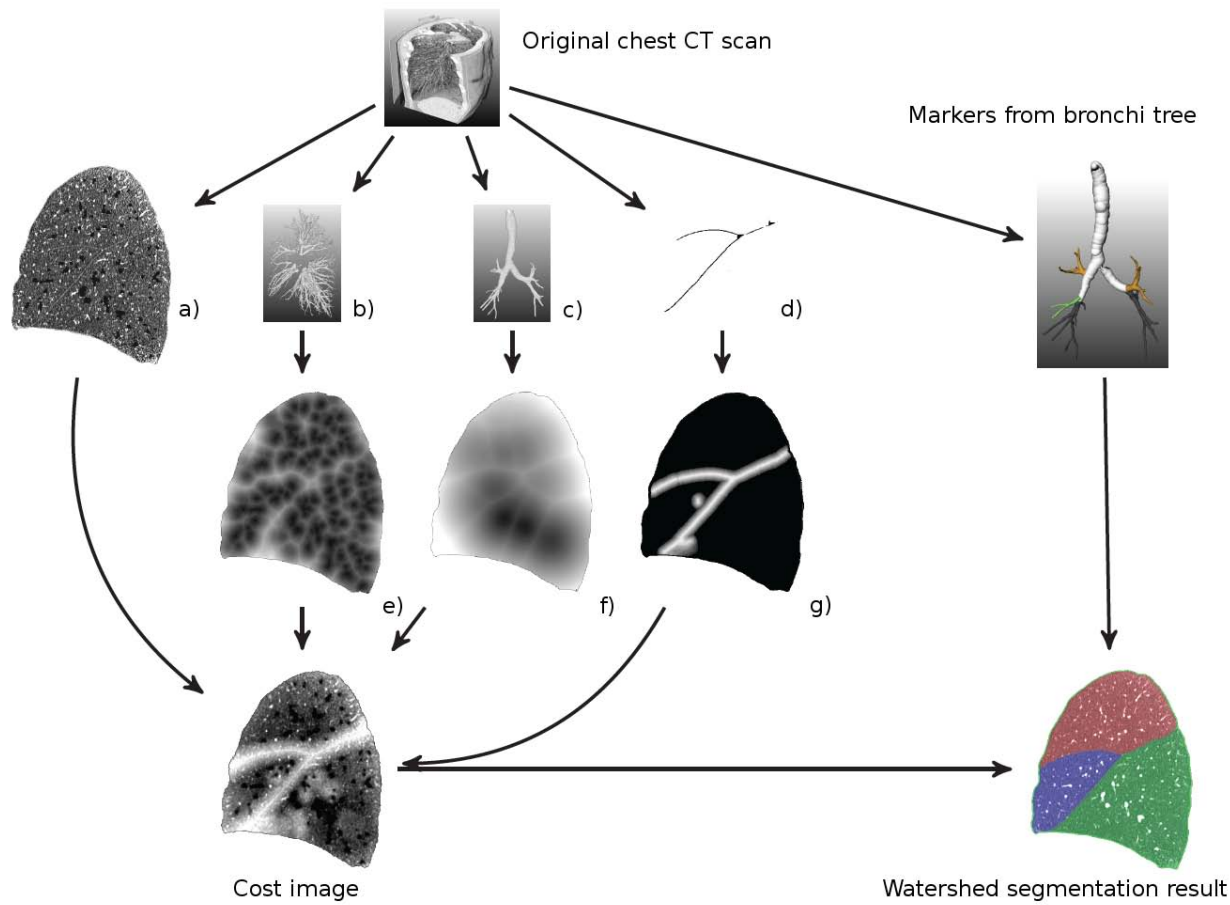

Fig. 3: Schematic diagram of the automatic lobe segmentation algorithm. From the original chest CT scan four features are extracted to calculate the cost image for the watershed transformation: a) the original data with the blood vessels masked out b) the pulmonary vasculature c) the bronchial tree and d) the pulmonary fissures. A distance transformation is calculated from e) the vasculature, f) the bronchial tree and g) the fissures (inverted and squared) to get local maxima at the lobar boundaries. All four inputs are equally weighted to obtain the cost image for the watershed transform. Markers for the lobes are calculated automatically from the bronchial tree.

vasculature is sufficient. There is high contrast between blood vessels and lung parenchyma that enables a coarse segmentation of the pulmonary blood vessels by thresholding the data inside the lung region. The goal is to include as many vessels as possible but exclude fissures and other dense structures.

Before thresholding a downscaling with clamping is applied to reduce memory requirements. With the following equation the dataset v_{orig} is scaled down to the 8-bit range [0, 255], where 255 marks voxels outside the lung mask L:

$$v_{ds} = \begin{cases} max(0, min(254, \frac{v_{orig}+1024}{4})) & v \in L \\ 255 & otherwise. \end{cases} \quad (1)$$

The resulting dataset v_{ds} is thresholded to receive the vesselmask V.

$$V = 130 \leq v_{ds} < 255. \quad (2)$$

The fixed threshold of 130 ($\widehat{=}$ 504 HU) was empirically estimated on an independent dataset and proved to be a good tradeoff between sensitivity and specificity.

After the thresholding, a connected component analysis filters out structures with a volume of less than 2 ml to separate the interconnected vasculature from smaller, isolated high-density structures such as thickened parts of the fissures.

2) Pulmonary fissures: The first step of the fissure segmentation process is an enhancement of the fissures based on the eigenvalues of the Hessian matrix that gives a fissure probability for each voxel. The relation between the eigenvalues $|\lambda_1| \leq |\lambda_2| \leq |\lambda_3|$ of the Hessian matrix $\mathbf{H}$ describes the local image structure [5]. In this work, $\mathbf{H}$ is calculated using a derivative-of-Gaussian approach with $\sigma = 1.0$ mm. Fissures can locally be modeled as a sheet where the eigenvalue orthogonal to the fissure plane is large, and the other two eigenvalues are small. Thus, on the bright fissures, the ideal relationship is defined as $|\lambda_1| = |\lambda_2| = 0$ and $\lambda_3 \ll 0$.

The here presented fissure enhancement approach characterizes fissure voxels as follows: $0 \ll |\lambda_3| < \delta$ and $|\lambda_2| \approx 0$, where δ describes the $|\lambda_3|$ value for vessels. δ is introduced to discriminate between fissures and vessels since vessels usually exhibit a larger $|\lambda_3|$ compared to fissures because of their stronger image contrast. From these characteristics two

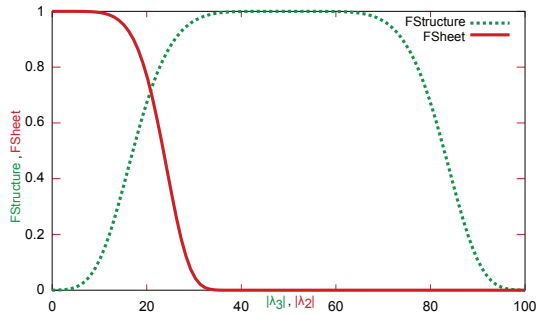

Fig. 4: Plot of $F_{Structure}$ and F_{Sheet}. X-axis refers to $|\lambda_3|$ for $F_{Structure}$ and to $|\lambda_2|$ for F_{Sheet}.

features are derived (Fig. 4):

$$F_{Structure} = \Theta(-\lambda_3) e^{\frac{-(\lambda_3-\alpha)^6}{\beta^6}} \tag{3}$$

$$F_{Sheet} = e^{\frac{-\lambda_2^6}{\gamma^6}}. \tag{4}$$

$F_{Structure}$ rates the strength of image structure. Because the intensity of the fissure structure varies both between patients and also within a single dataset, a wide interval of intensities for high fissure probability is defined. This is done by calculating the sixth power which results in a smoothed rectangular-like curve (see Figure 4). In order to estimate suitable values for α and β we analyzed $|\lambda_3|$-values of five datasets with given fissure and vessel mask that were not used for evaluation in this paper. The analysis revealed that fissure voxels show $|\lambda_3|$-values between 20 and 80. Vessels show much higher $|\lambda_3|$-values but the $|\lambda_3|$-values of small vessels can go down to around 60. Since we prefer sensitivity over specificity we choose $\alpha = 50$ and $\beta = 35$ for the distribution function of $F_{Structure}$. Thereby, voxels with a $|\lambda_3|$-value between 30 and 70 are assigned a high fissure probability whereas voxels with a $|\lambda_3|$-value $\gtrsim 100$ are excluded from the fissure segmentation (see Figure 4). False positive results are discriminated later by combination with the F_{Sheet} feature. The term $\Theta(-\lambda_3)$ describes a heaviside function that sets $F_{Structure}$ to 0 for voxels with $\lambda_3 \geq 0$, i.e., a dark structure on a bright background is not a fissure.

The F_{Sheet} feature discriminates between a sheet structure and other structures such as nodules or vessels, as these latter structures have larger $|\lambda_2|$ values. γ is empirically set to 25 by investigating typical values for fissures and other high-contrast structures within the lungs of the five test datasets not used for evaluation of this paper. Thus all voxels with a $|\lambda_2|$ value $\gtrsim 30$ are assigned to a probability of 0 and are therefore excluded from the fissure segmentation (see Figure 4). $F_{Structure}$ and F_{Sheet} are in the range $[0, 1]$. The two features are combined to the overall fissure similarity measure $S_{Fissure}$:

$$S_{Fissure} = F_{Structure}\, F_{Sheet}. \tag{5}$$

The result of the fissure enhancement is for each voxel a fissure similarity value between 0 and 1. An example of fissure enhancement can be seen in Figure 5b.

The result of the fissure enhancement are converted to a segmentation of the lobar fissures that are required as input

(a) Original data. (b) Fissure Enhancement. (c) Fissure Segmentation.

Fig. 5: Axial view of the two-step fissure segmentation for LOLA11 case 1.

for the watershed lobe segmentation. A mask C is constructed which describes all candidate fissure voxels that fulfill two constraints. The first constraint is a minimal fissure similarity $S_{Fissure}$ and the second constraint demands an intensity value in a defined range:

$$C = [S_{Fissure} > 0.1\ ] \wedge [I_v < (\mu_{vessel} - 2\sigma_{vessel})], \tag{6}$$

where μ_{vessel} and σ_{vessel} are the mean intensity and standard deviation of vessel voxels, respectively. These parameters are estimated individually for each CT scan by a histogram analysis of the segmented vessels (see Section II-A1). The purpose of the gray value information is to exclude vessels which usually have higher intensities than fissures and are not already excluded by $F_{Structure}$.

The resulting mask C contains spurious responses on small plate-like structures. To obtain the final fissure segmentation we use a vector-based connected-component analysis. The largest eigenvalue of a sheet is perpendicular to the plane. Thus, the corresponding eigenvector of the largest eigenvalue shows the orientation of a structure. The curvature of a fissure is locally low, so adjacent fissure voxels have similar largest eigenvectors. Taking advantage of this property, a 3D vector-based connected component analysis with a 6-neighborhood is applied on the candidate voxels in C, similar to van Rikxoort et al. [10]. The similarity is calculated by the inner product of the normalized eigenvectors, so that the inner product is 1 for identical vectors. Since pulmonary fissures are usually slightly bent, the inner product for fissure voxels can be slightly smaller than 1. Empirical analysis showed good fissure segmentation results for joining adjacent voxels inside mask C with an inner product ≥ 0.98 to a connected component. All 3D components with a volume of at least 0.1 ml are kept to obtain all significant fissure parts and remove most of the noise. Afterwards, a morphological closing with a cubic kernel of 3 x 3 x 3 voxels is applied to close minor gaps. Figure 5c shows an example of a fissure segmentation result.

3) Bronchi: Since each lobe is separately supplied by subtrees of the bronchial tree, distance to the bronchi is a suitable feature to detect lobar boundaries, similar as for the vessels. In CT images, the airway lumen is dark and separated from the parenchymal tissue by thin airway wall structures that appear brighter. Segmentation of the airways in CT images is challenging because often the parenchymal fissures have similar HU values as the lumen, and both partial volume effect (PVE) and noise obscure the airway walls. We apply two preprocessing steps to mitigate these problems and to facilitate

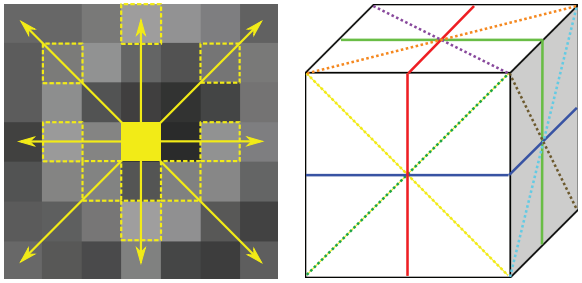

(a) From the center voxel the maximum intensities (dotted border) are calculated for all of the 8 rays (yellow arrows).

(b) Nine cutting planes in which the ray casting is applied.

Fig. 6: Bronchi enhancement filter.

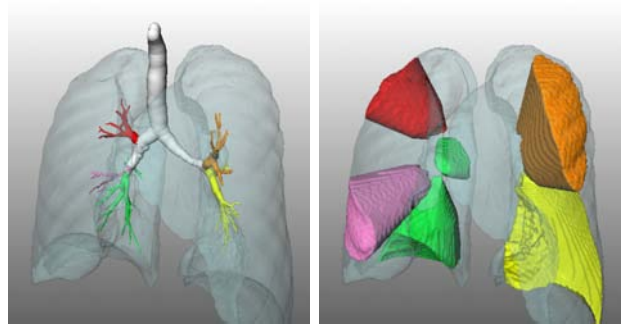

(a) Analyzed airway tree

(b) Lobar cones

Fig. 7: Result of the bronchi segmentation after lobar bronchi analysis (a) and the resulting lobar cones (b) that are used for lobe marker generation.

the segmentation of the bronchi. First, to reduce noise, a Gaussian smoothing with fixed kernel width ($\sigma = 1.0$ voxel) is applied to the image although the blurring increases the partial volume related problems.

Second, a bronchi enhancement filtering is applied to the blurred image. Partial volume effects and the additional Gaussian blurring let the lumen of small airways appear brighter than normal air. The goal of the bronchi enhancement filtering is to detect voxels that are surrounded by dense circular structures as bronchi and to revert these volume averaging effects by decreasing their density again. For bronchi that are orthogonal to the axial plane the following approach enhances bronchi voxels. For each voxel the maximum intensities max_{a-h} for 8 homogeneously distributed inplane rays with a length of 3 voxels are calculated (see Figure 6a). The following equation provides high values for bronchi voxels $bronchi_{bright} = avg(max_{a-h}) - Var(max_{a-h}) - v_{orig}$. Including the variance ensures that only voxels that are evenly surrounded by bright voxels are enhanced. And the subtraction of the original image v_{orig} suppresses filter responses in homogenous dense regions. Since only a few bronchi are orthogonal to the axial plane this process is repeated for 8 more planes: sagittal, coronal, and 6 diagonal planes (see Figure 6b). Only the planes that cut through the bronchi show high responses. Thus, from the 9 filter responses $bronchi_{bright1-9}$ the average of only the 3 largest responses is calculated and set as the voxel value in the enhancement image. In the last step the enhancement image is subtracted from the original image to get dark values inside the bronchi.

A 3D region growing algorithm is used to extract the airway lumen from the preprocessed image. The region growing is initialized by detecting the trachea. A 2D connected component analysis of the airspace mask finds trachea candidates and the components that overlap in z-direction are selected to be the trachea [23]. Starting from the position of the minimum gray value within the trachea, the segmentation threshold is iteratively increased and the segmentation volume is monitored. The steepest slope of the observed threshold-volume-curve within the interval of $10 - 150$ ml is searched and the threshold below this step is used as the final region growing threshold.

In images with high noise levels, this segmentation mask is likely to contain holes, especially in the larger airways. Since this may negatively impact subsequent graph construction, a second segmentation mask is created from the original CT data specifically for segmenting large airways. For each voxel, the average of minimum and maximum voxel intensities within a resolution-dependent neighborhood (2/1/0 voxels in each direction for an image resolution of $\leq$1mm/$\leq$3mm/$>$3mm) is calculated. Afterwards, the same iterative region growing as before is applied with slightly decreased thresholds of $5 - 100$ ml. The segmentation masks are then combined with a union operation.

While the analysis of the threshold-volume curves is able to detect larger leaks in almost all cases, smaller leaks may still be present in some region growing results. In order to remove these, local structure sizes are estimated by means of a Euclidean distance transform of the segmentation mask and compared to the size of their smallest connection to the carina. All voxels exceeding a ratio of 1.4 between distance to the segmentation boundary and their connectivity to the carina are considered as leaks, and a dilation of these voxels is removed from the segmentation mask. This is similar to the leak detection stopping criteria used in many tree-oriented wavefront propagation segmentation methods as e.g. [24].

B. Watershed-based lobe segmentation

The anatomical information of fissures, bronchi, and vessels are combined into a cost image for a watershed-based lobe segmentation. For the 3D marker-based watershed transformation two kinds of inputs are required: a cost image and markers corresponding to the five lobes (see Figure 3). To obtain these inputs for a chest CT scan in which the vessels, fissures, and bronchi have been segmented the following steps are performed: 1) the segmentations are combined into a cost image, 2) markers for the watershed are computed, and 3) the lobes are segmented using a 3D watershed transformation and post processing is applied.

1) Cost image construction: An ideal cost image for the watershed transformation used for lobe segmentation shows local maxima at the lobar boundaries and low values within the lobes. The cost image is constructed using four features. The

first feature is derived from the segmentation of the vascular tree. The rationale for using the vascular tree is that there are usually few vessels near the lobar borders, therefore, a Euclidean distance to the vessels is calculated for each voxel in the lung. The normalized result is a feature image V_{cost} in the range of [0, 255] that shows high values in the region of the lobar boundaries, see Figure 3e for an example. The second feature is derived from the segmentation of the bronchial tree. Since the lobes are supplied by separate subtrees of the bronchial tree there are no bronchi near the lobar borders. As for the vessel-based feature, a Euclidean distance to the bronchi is computed and normalized for each voxel in the lungs, leading to a feature image B_{cost} in the range of [0, 255] with high values near the lobar borders (Figure 3f). The third feature is derived from the segmentation of the fissures. Since the fissures are the physical boundaries between the lobes, on locations where they are present they indicate the exact lobar boundary and should be emphasized. To obtain the feature the Euclidean distance from the fissures in a region of 2 cm around the fissures is calculated. Thereby the fissures are emphasized and gaps in the fissure segmentation can be bridged. The result image v contains zeros at the detected fissures. Thus, to get the feature image F_{cost} in the range of [0, 255] with high values at the fissures, v is squared, inverted, and normalized:

$$F_{cost} = 255 \cdot \left(1 - \left(\frac{v}{v_{max}}\right)^2\right), \tag{7}$$

where v_{max} is the maximum value of the image v.

The last feature is based on the observation that due to the small σ (= 1mm) of the fissure enhancement filter pathological thick fissures are not always detected by the fissure segmentation. In high-resolution chest CT scans the fissures, and especially pathological thick fissures, show higher density than the surrounding lung parenchyma. Thus the fourth feature O_{cost} is the original CT scan v_{orig}, normalized and clamped to the range [0, 255] (see Figure 3a). The vasculature is masked out since vessels usually show even higher density than thick fissures:

$$O_{cost} = \begin{cases} max(0, min(255, \frac{v_{orig}+1024}{4})) & \notin V \\ 0 & otherwise. \end{cases} \tag{8}$$

In order to obtain the final cost image, the four features are combined with equal weight (see Figure 3).

$$Cost = \frac{V_{cost} + B_{cost} + F_{cost} + O_{cost}}{4}. \tag{9}$$

By combining the four input features false positive responses of individual features are reduced since those areas that have a high value in all individual cost images are enhanced.

2) Markers for the watershed segmentation: Markers should ideally be created equally distributed throughout the lobes to get a good coverage of the lobe areas. To generate the markers, the different subtrees belonging to the lobes and lobar segments are identified in the airway tree. This is done by searching for major bifurcations separating large subtrees in appropriate orientations (see Figure 7a). In the first step a directed graph is modeled from the bronchi tree with the trachea as root [25]. The center of gravity and volume of the segmented voxels are calculated for each subtree. Then, for each pair of sibling subtrees the following separation score is calculated:

$$(\overrightarrow{n} \cdot \overrightarrow{d})^2 \cdot min(w_1, w_2), \tag{10}$$

where $\overrightarrow{n}$ is the offset between the two subtrees centers of gravity. $\overrightarrow{d}$ is the particular separation direction for the lungs, lobes, and segments, that describes the typical topology of the lungs. Thus, it is the expected direction between the two lungs, two particular lobes, or two particular segments that is determined beforehand on a set of pilot data. w_1, w_2 are the volumes of the two subtrees and $min(w_1, w_2)$ gives the volume of the smaller subtree and discriminates large subtrees against small subtrees. The two subtrees with the maximum separation score are separated into different branches. In this way first the bronchial tree is divided and labeled into left and right lung and then these subtrees are further divided into the lobes and segments.

The labeled airway tree can now be used to determine marker positions for the watershed. However, since the segmentation of the airway tree does not reach the periphery of the lungs and the length of the airways detected is not consistent between scans, the segmentation of the airways is not directly usable to determine marker positions. To overcome this problem, areas in the lung mask to place watershed markers are identified based on the labeled airway tree as follows. For each lobe the center of gravity of all terminal branch positions is calculated. A plane is created that runs through the center of gravity, with the normal vector of the plane pointing to the root of the subtree. The connection lines from each terminal branch position to the root position are intersected with this plane and a principal component analysis is performed for the intersection points. An ellipse is created from the two principal components. Based on this ellipse and the root of the subtree a cone is defined for each pulmonary lobe (see Figure 7b). To compensate for varying segmentation depths between the lobes, the cones are extended from the plane to the lung boundary with half their original aperture. In cases where cones from different lobes overlap, the overlap areas are removed from both cones.

The superior segment of the right lower lobe is handled with a separate cone because it cannot always be represented by a single lower lobe cone appropriately. Figure 7 shows an example of the labeled bronchi and resulting cones. All bronchi and vessels inside the cones are assigned to the corresponding cone label. In the next step the labeled vessels and the bronchi are automatically converted into 3D markers for the watershed segmentation. To delimitate the numbers of markers the image resolution is temporarily set to 4.5 mm x 4.5 mm x 4.5 mm which results in 3000-4000 markers for each lung.

3) Lobe segmentation and post processing: To obtain a lobe segmentation from the cost image $Cost$ and the markers, the 3D watershed transformation proposed by [26] is performed. Downsampling of the cost image to a resolution of 1.5 mm x 1.5 mm x 1.5 mm is applied to reduce calculation time. The applied watershed algorithm separates regions with local maxima in between and can be used with an arbitrary number

of markers.

The borders between the obtained lobes after the watershed segmentation are not always smooth due to local variations in the cost image. Two majority filters with different kernel sizes (3x3x3 and 5x5x1) are applied in a row to smooth the boundaries. The label value that occurs most often under the kernel is set to the voxel. To obtain the lobe segmentation on the original resolution, the segmentation results are upsampled using nearest neighbor interpolation.

III. Data

Two datasets were used for evaluation. Dataset 1 allows direct comparison to [11], Dataset 2 is publically available.

A. Dataset 1

Dataset 1 contains 20 normal dose (120 kV, 100-150 mAs) inspiration CT chest scans that were used in [11] to evaluate the lung lobe segmentation method. The scans are of 20 different patients from the University Medical Center Utrecht, The Netherlands. The inplane resolution is between 0.54 mm and 0.71 mm whereas the slice thickness is between 0.7 mm and 1.0 mm. A human observer manually indicated the lobar fissures to allow quantitative evaluation. The observer was instructed to indicate the visible fissure on every fourth coronal slice. For details we refer to [11].

B. Dataset 2

Dataset 2 was taken from the lung and lung lobe segmentation challenge LOLA11 [3]. There are 55 CT scans from a variety of clinically common scanners and protocols including many cases with severe pathologies. The inplane resolution is between 0.53 mm and 0.78 mm whereas the slice thickness is between 0.3 mm and 1.5 mm.

The organizers of LOLA11 have available a manual segmentation of the lung lobes on 9 coronal slices for each case by two human observers. Both observers were instructed not to draw a lobar border when they felt it was not possible. This led to two scans for the left major fissure where no lobar border was defined (cases 21 and 45), one for the right major fissure (case 44), and five for the right minor fissure (cases 21, 44, 45, 48, and 55). For one scan, case 52, observers disagreed about which fissure was the right minor fissure, leading to a mean distance of 85.11 mm. The reference segmentations can not be downloaded, but the LOLA11 challenge is still open. Participants can upload segmentation results to receive evaluation results.

Since lobar segmentation is most challenging in cases with incomplete fissures we analyzed the segmentation results with respect to the fissure completeness. For all cases of dataset 2 we quantified the fissure completeness for the left major, right major, and left minor fissure with the method presented in van Rikxoort et al. [27]. The fissure completeness is described as a value in the range from 0 to 1.

IV. Experiments & results

The presented method is implemented in the software development environment MeVisLab [28][29].

TABLE I: Results of Experiment 1. The average mean and maximum distance from the manually drawn fissure to the automatically found lobe border are calculated for dataset 1. For comparison the results of the methods by van Rikxoort et al. [11] and Kuhnigk et al. [12] are shown.

Fissure	Average ± std of case mean (mm)		Average ± std of case max (mm)	
left major	**0.69** ±	0.89	11.26 ±	5.98
left major (Rikxoort [11])	**0.48** ±	0.15	10.30 ±	3.52
left major (Kuhnigk [12])	**3.22** ±	3.60	24.77 ±	18.88
right major	**0.67** ±	0.58	12.40 ±	4.12
right major (Rikxoort [11])	**1.23** ±	0.24	9.96 ±	2.89
right major (Kuhnigk [12])	**2.06** ±	1.45	17.65 ±	7.24
right minor	**1.21** ±	1.52	11.63 ±	12.53
right minor (Rikxoort [11])	**1.28** ±	0.53	9.59 ±	7.38
right major (Kuhnigk [12])	**3.08** ±	1.14	15.21 ±	5.93
overall	**0.86** ±	1.00	11.76 ±	7.54
overall (Rikxoort [11])	**1.00** ±	0.31	9.95 ±	4.60
overall (Kuhnigk [12])	**2.78** ±	2.06	19.21 ±	10.68

A. Experiment 1

The presented lung lobe segmentation approach was applied to dataset 1. The mean and maximum distance from the manually drawn reference were calculated for each lobar border in 3D by computing the distance between each voxel in the reference standard and the closest voxel in the lobar segmentation. Table I shows the results of Experiment 1 with a direct comparison to the results of a recently published method by van Rikxoort et al. [11] and the preliminary approach of the here presented method presented by Kuhnigk et al. [12]. Furthermore, Figure 8 shows screenshots of 6 cases with the overlayed lobe segmentation result. It can be seen from Table I that the proposed method performs well on dataset 1, with better performance than the method by Kuhnigk et al. and van Rikxoort et al. overall.

B. Experiment 2

In Experiment 2 we applied the presented lung lobe segmentation method to dataset 2 and submitted the resulting segmentations to the LOLA11 challenge [3]. The evaluation metric of LOLA11 is the volume overlap to the manual reference segmentation of one observer. In addition, a total score is calculated from the average overlap of the five lobes. Currently, the presented method has the highest score (0.88) in the LOLA11 challenge (see [30]). Van Rikxoort et al. also submitted the method presented in [11] to LOLA11 and got a score of 0.85. Table II shows the overlap results for dataset 2.

For cases with a poor lung segmentation, the volumetric overlap can be low even if the detection of the lobar border is completely correct. Therefore, the same measurements as in Experiment 1 were computed solely around the fissures. Since at locations where there is no fissure the lobar boundary is not exactly defined, in the LOLA11 challenge a slack border of 2 mm was taken into account for evaluation. This means that every voxel within 2 mm of the manually drawn lobar border is assumed to have a distance of 0. Table III shows

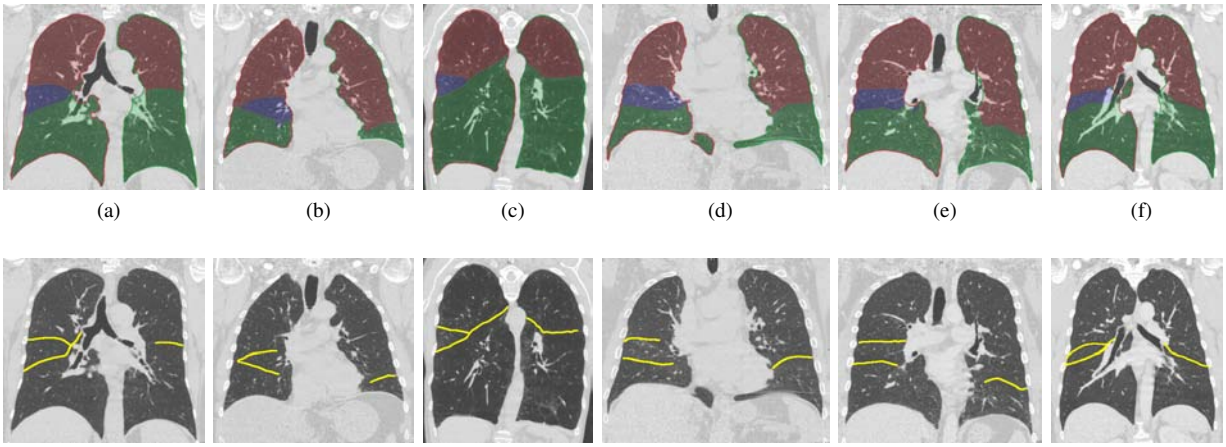

Fig. 8: Coronal screenshots of 6 cases of Experiment 1. The upper row shows the segmentation results (red = upper lobes, blue = middle lobe, green = lower lobes) and the lower row shows the reference segmentation (yellow).

TABLE II: Volumetric overlap results of Experiment 2. The mean, standard deviation (SD), minimum (min), maximum (max), and median overlap to a manual reference segmentation are computed for dataset 2. LUL = left upper lobe, LLL = left lower lobe, RUL = right upper lobe, RML = right middle lobe, RLL = right lower lobe.

Lobe	mean	SD	min	max	median
LUL	**0.92**	0.16	0.20	1	0.98
LLL	**0.89**	0.23	0	1	0.96
RUL	**0.92**	0.09	0.60	1	0.96
RML	**0.77**	0.30	0	0.99	0.89
RLL	**0.91**	0.18	0	1	0.97
LOLA score	**0.88**				

the average distance for all cases of dataset 2. Since outliers have a strong effect on the average distance, Table III also shows the median distances to the lobar borders. In addition, 21 coronal screenshots of segmentation results are depicted in Figure 9 and 3D renderings of the same datasets are depicted in Figure 10. Axial and sagittal screenshots of four cases are shown in Figure 11.

C. Experiment 3

Figure 12a shows the relation between fissure completeness and mean distance to the reference for all three fissures of the 55 cases from the LOLA11 dataset. Since incomplete fissures can lead to locally inaccurate lobar border segmentation the relation between the fissure completeness and the maximum distance to the reference is plotted in Figure 12b. It can be seen in Figure 12 that there is no clear relation between fissure completeness and the performance of the method. For both results the same slack border of 2 mm as described in Experiment 2 was used. We can conclude that the performance of the method is not substantially compromised by fissural incompleteness.

V. Discussion and Conclusion

This paper presented a lobe segmentation method that combines information from automatic segmentations of the lungs, fissures, vessels, and bronchi to segment the lobes. The approach is anatomically inspired and similar to the way humans determine the lobar boundary. Visible fissures are used for segmentation because they are the most precise feature, but in absence of a fissure, the vessels and airways become more important. Vessels are distributed all over the lung and due to the high contrast to the lung parenchyma a good segmentation of the vessels is feasible. But in some cases vessels cross the lobar boundaries. Thus, the assumption that there are no vessels at the lobar boundary is not always correct. In contrast a deep segmentation of the bronchi is challenging but there are definitely no bronchi at the boundary between the lobes. By combining the information of different anatomical structures we expect to get as much as possible information to perform an accurate lobe segmentation.

Automated segmentation of anatomical structures is challenging in cases with abnormalities. By combining information from several structures the method becomes more robust against a failed segmentation of one of these structures. Most previously published methods heavily rely on the detection of the fissures, which is less reliable, especially in cases with abnormalities such as shown in Figure 9o - 9u. Another method reported in literature [11] that combines information from different structures (the lungs, fissures, and bronchi) uses an atlas-based approach. A disadvantage of that method is that it can only produce lobar shapes close to the shapes represented in the atlases, which leads to failures in cases where pathological processes had altered the lobe shapes. The method presented in this paper can generate any lobar shape based on the input segmentations.

The presented approach was evaluated on 75 scans in total with varying degrees of pathologies and fissure completeness. The results show that the method performs well in almost all cases and is robust against incomplete fissures. Several

TABLE III: Distance measurement results of Experiment 2. The average as well as the median of the mean and maximum distance from the manually drawn lobar borders for all cases of dataset 2 are shown.

Fissure	average of case mean (mm)	average of case max (mm)	median of case mean (mm)	median of case max (mm)
left major	**0.98** ± 1.45	16.60 ± 21.33	**0.47**	9.95
right major	**3.97** ± 21.86	15.86 ± 25.88	**0.48**	9.73
right minor	**3.09** ± 20.83	6.90 ± 23.43	**0.06**	3.00
overall	**2.68** ± 14.71	13.12 ± 23.55	**0.34**	7.56

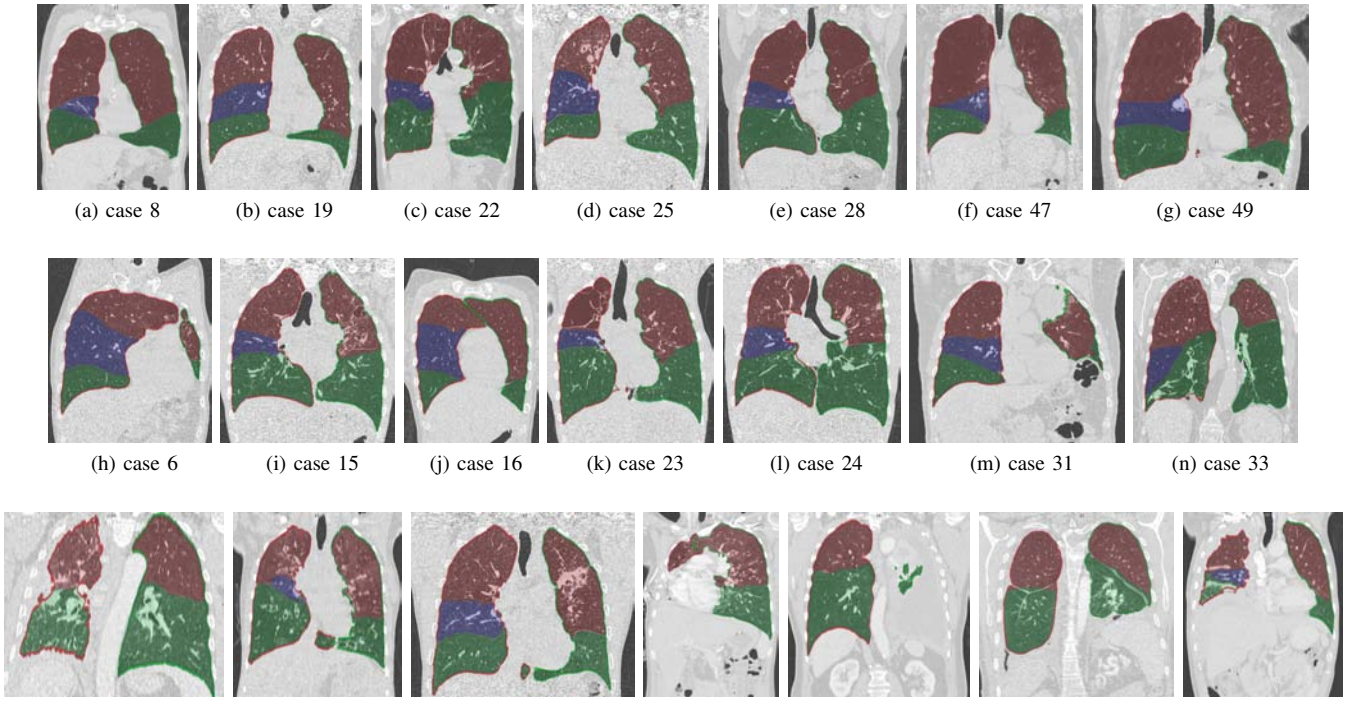

(a) case 8 (b) case 19 (c) case 22 (d) case 25 (e) case 28 (f) case 47 (g) case 49

(h) case 6 (i) case 15 (j) case 16 (k) case 23 (l) case 24 (m) case 31 (n) case 33

(o) case 35 (p) case 37 (q) case 42 (r) case 44 (s) case 45 (t) case 48 (u) case 50

Fig. 9: Coronal screenshots of 21 segmentation results of Experiment 2 (red = upper lobes, blue = middle lobe, green = lower lobes). The first row shows relatively easy cases with normal anatomy and no more than mild pathologies. The second and third row show more challenging cases with abnormal anatomy or severe pulmonary diseases.

approaches for automatic lung lobe segmentation have been published, as presented in Section I. Comparison of the performance of different approaches was difficult so far since the approaches were evaluated on different datasets and regarded different validation criteria. In this paper we compared the here presented lung lobe segmentation method to two other recently published approaches [11] [12] and performed an evaluation on publically available data.

In Experiment 1 the presented method is compared to the methods presented in [11] and [12] on 20 cases with mild pathologies. The results show that our segmentation method performed well for 20 cases with mild pathologies. The results are comparable to the results of the method by van Rikxoort et al. [11]. Our method shows slightly superior results for the right major fissure and slightly inferior results for the left major fissure. The results for the right minor fissure are very comparable. The performance of our method is superior to the results of the method presented in [12], with an average distance to the fissure of 0.86 mm compared to 2.78 mm. The method in [12] can be seen as the preliminary approach of the here presented method. It also employs a watershed transformation but incorporates only information of the vessels for the calculation of the cost image. Thus, adding the information from fissures and bronchi improved the segmentation result.

Experiment 2 presents an evaluation on publically available data provided by the lung and lung lobe segmentation challenge LOLA11 [3]. In contrast to the cases of Experiment 1, these 55 CT scans include cases with severe pathologies. All of the papers in literature evaluated lung lobe segmentation methods on data with mild pathologies. This is the first paper with an evaluation of severely abnormal data (see Figure 9). Currently only two groups participated in LOLA11 but the contest is still open. Experiment 2 shows that the performance of the here presented lobe segmentation method with a LOLA11 score of 0.88 is slightly better than the one by Rikxoort et al. with a LOLA11 score of 0.85.

Table 3 provides the mean distances to the lobar borders for

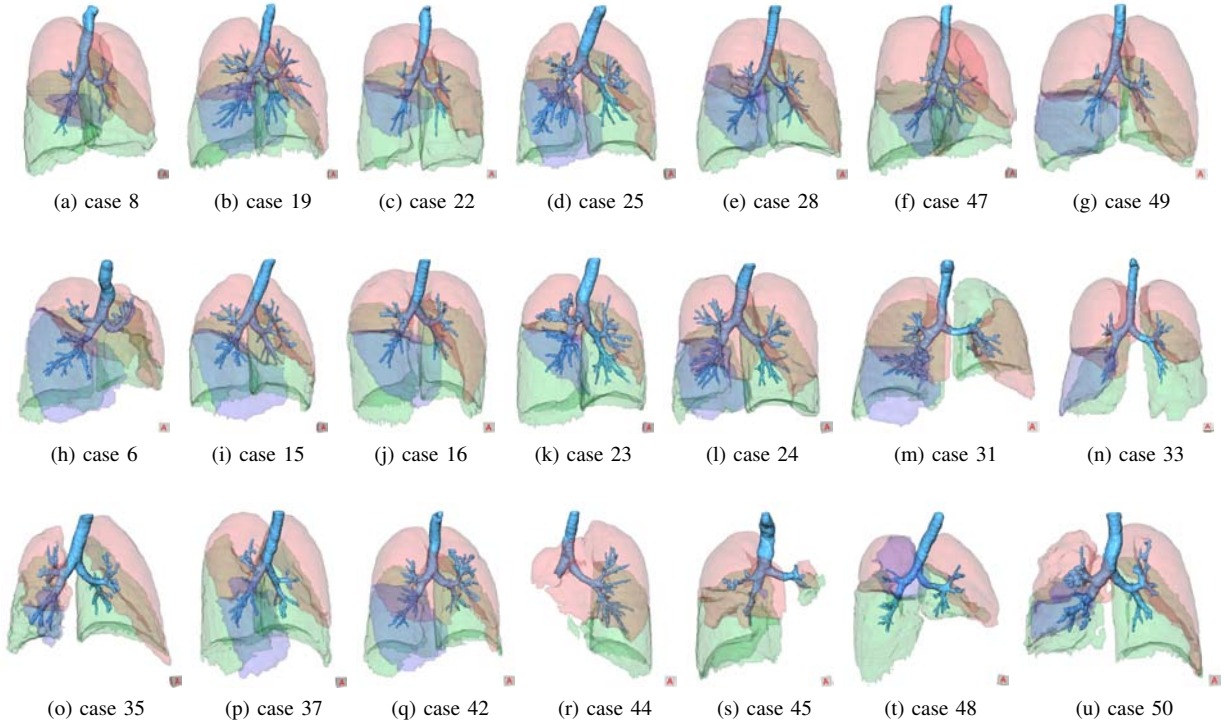

Fig. 10: 3D screenshots of 21 segmentation results of Experiment 2 (red = upper lobes, blue = middle lobe, green = lower lobes). The first row shows relatively easy cases with normal anatomy and no more than mild pathologies. The second and third row show more challenging cases with abnormal anatomy or severe pulmonary diseases.

the LOLA11 dataset. The values are on average higher than in Experiment 1. This has two causes. First, in Experiment 1 only visible fissures were taken into account for the reference standard while in Experiment 2 the lobar borders were defined also on locations of incomplete fissures. Second, dataset 2 contains more cases with severe pathologies.

Table III shows high standard deviation values for the mean distance of the right major and right minor fissure. Furthermore, the median values are substantially lower than the mean values (see Table III). The reason for the high mean values and the high standard deviation is that the segmentation of the right lobes for case 2 of LOLA11 completely failed because an artifact stopped the bronchi segmentation in the mediastinum (see Figure 13). In consequence no watershed markers at all could be calculated and the lobe segmentation stopped. In spite of the absence of resulting lobar boundaries, the distance was calculated and resulted in 152 mm for the right major fissure and 161 mm for the right minor fissure with a strong effect on the mean values of Table III. Excluding case 2, the average mean distance in Table III would improve to 1.00 mm $\pm$ 1.70 mm (before: 3.97 mm $\pm$ 21.86 mm) for the right major fissure and to 0.23 mm $\pm$ 0.41 mm (before 3.09 mm $\pm$ 20.83 mm) for the right minor fissure. It can be seen in Figure 13 that for case 2 of LOLA11 the segmentation of the lobes in the left lung was also unsatisfactory due to inadequate bronchi segmentation and labeling. However, since at least some bronchi markers are placed, a lobar segmentation was produced leading to lower distances then at the right lung.

The here presented approach took on average 10 minutes for one case of this experiment on a single core of a 2 years old standard PC. The largest amount of time is needed by the fissure segmentation algorithm. A downsampling was applied in several steps to reduce computation time which might have minor effects on the segmentation quality. The approach is not yet optimized for speed and for future work the processes can be parallelized. After optimization the approach could be applied on full resolution. The approach of van Rikxoort et al. took 110 minutes on average for one case of this experiment.

Several publications focus on datasets with incomplete fissures [11] [16] [14] because the completeness of fissures can impede the quality of lung lobe segmentation. Therefore, in Experiment 3 we analyzed the relation between fissure completeness and the segmentation quality. Figures 12a and 12b show that the fissure completeness does not obviously impact the distance from the calculated lobar boundary to the reference segmentation. To pick two example data, case 24 (see Figure 9l) has a fissure completeness of only 0.21 for the right minor fissure but the calculated mean distance to the reference segmentation is also low with 0.13 mm. An example with a high fissure completeness of 0.87 for the right major fissure and a poor segmentation result of a mean distance of 161.17 mm is case 2. The bronchial segmentation for this case failed because of the presence of a strong artifact in the scan and no lobes were calculated at all (see Figure 13). In general, Experiment 3 shows that the here presented lung lobe segmentation approach is robust against incomplete fissures.

Results of Experiment 2 show a strong dependency to the segmentation quality of the bronchi. Thus, for future work

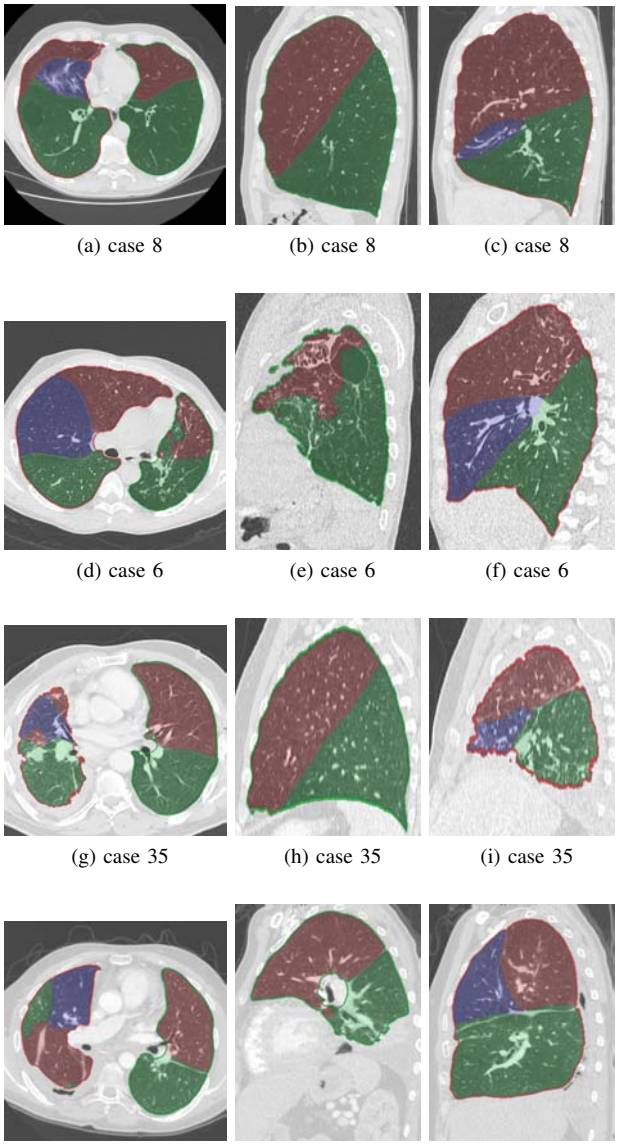

(a) case 8 (b) case 8 (c) case 8

(d) case 6 (e) case 6 (f) case 6

(g) case 35 (h) case 35 (i) case 35

(j) case 48 (k) case 48 (l) case 48

Fig. 11: Axial (a, d, g, j) and sagittal screenshots of the left (b, e, h, k) and right (c, f, i, l) lung for four cases of Experiment 2. Red = upper lobes, blue = middle lobe, green = lower lobes.

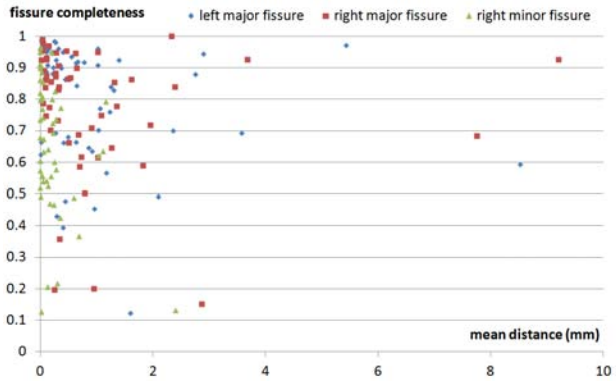

(a) Mean distance to the reference.

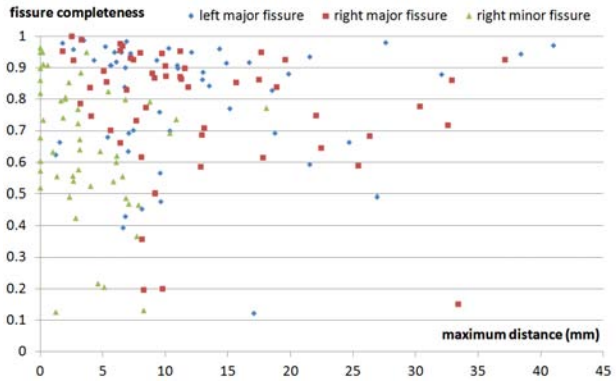

(b) Maximum distance to the reference.

Fig. 12: Relation between fissure completeness and the distance to the reference segmentation. Both plots are cropped to optimally illustrate the majority of the data. Thus, 2 outliers in a) (at distance 152/0.79 and 161/0.87) and 5 outliers in b) (at distances 54/0.66, 85/0.64, 130/0.96, 172/0.79, and 191/0.87) are not depicted.

we will focus on minimizing the dependency to the bronchi segmentation quality. In the current version no watershed-based lobe segmentation can be performed in case of a failed bronchi segmentation because the required lobe markers are generated from the labeled bronchi tree. One idea is to heuristically set lobe markers based on their position in the lung in case of a failed bronchi segmentation. An alternative would be to apply a coarse registration with a labeled lung to obtain the lobe markers.

Furthermore, pathological thick fissures are sometimes not detected as fissures but as vessels. Thus, for these cases the lobe segmentation does not exactly follow the lobar fissures (see Figures 9t and 9u). The weight of the fissures in the cost image is equal to the weights of the other inputs. Such a low weight allows a high degree of independence against missing fissures compared to a higher weight which can increase the accuracy of the segmentation. For future work we want to set the weight of the inputs of the cost image dynamically based on a confidence estimation of the vessel, bronchi, and fissure segmentation.

Moreover, our experiments and the results of other published lobe segmentation approaches (see Section I) show that due the the variation of lung anatomy and pulmonary diseases no automatic segmentation method can ensure a satisfying lobe segmentation result for all cases. Thus, another key point for future work is to implement an interactive method that allows fast and intuitive correction of a given segmentation result.

In conclusion, we have presented a fast automatic lobar segmentation method and shown in an extensive series of experiments with 75 CT scans that the method performs well and is robust against missing fissures.

References

[1] National Emphysema Treatment Trial Research Group, "Patients at high risk of death after lung-volumereduction surgery," *New England Journal of Medicine*, vol. 345, no. 15, pp. 1075–1083, 2001.

[2] M. Gülsün, O. Ariyürek, R. Cömert, and N. Karabulut, "Variability of the pulmonary oblique fissures presented by high-resolution computed tomography," *Surgical and Radiologic Anatomy*, vol. 28, pp. 293–299, 2006.

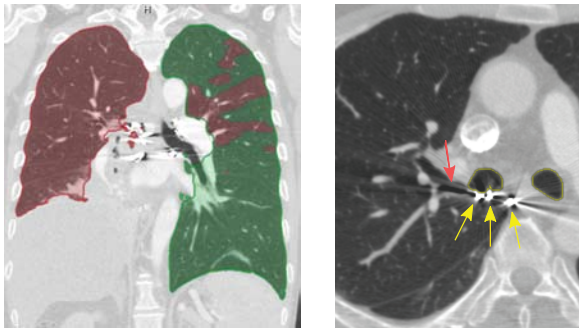

(a) Coronal view of the lobe segmentation result.

(b) Axial slice with artifacts.

Fig. 13: LOLA11 case 2. a) Segmentation result with no lobar boundaries in the right lung caused by artifacts that stop the required bronchi segmentation. b) The yellow arrows show the artifacts that stops the bronchi segmentation. The bronchi marked with the red arrow is not segmented.

[3] LOLA11, 2011, URL: http://lola11.com/.

[4] E. van Rikxoort, B. van Ginneken, M. Klik, and M. Prokop, "Supervised enhancement filters: application to fissure detection in chest CT scans," *IEEE Transactions on Medical Imaging*, vol. 27, no. 1, pp. 1–10, 2008.

[5] R. Wiemker, T. Buelow, and T. Blaffert, "Unsupervised extraction of the pulmonary interlobar fissures from high resolution thoracic CT data," *Computer Assisted Radiol. Surgery*, vol. 1281, pp. 1121 – 1126, 2005.

[6] J. Wang, M. Betke, and J. P. Ko, "Pulmonary fissure segmentation on CT," *Medical Image Analysis*, vol. 10, no. 4, pp. 530 – 547, 2006.

[7] J. Pu, J. Leader, B. Zheng, F. Knollmann, C. Fuhrman, F. Sciurba, and D. Gur, "A computational geometry approach to automated pulmonary fissure segmentation in CT examinations," *IEEE Transactions on Medical Imaging*, vol. 28, no. 5, pp. 710 –719, 2009.

[8] Q. Wei, Y. Hu, J. MacGregor, and G. Gelfand, "Automatic recognition of major fissures in human lungs," *International Journal of Computer Assisted Radiology and Surgery*, vol. 7, no. 1, pp. 111–123, 2012.

[9] F. C. Sciurba, A. Ernst, F. J. Herth, C. Strange, G. J. Criner, C. H. Marquette, K. L. Kovitz, R. P. Chiacchierini, J. Goldin, and G. McLennan, "A randomized study of endobronchial valves for advanced emphysema," *New England Journal of Medicine*, vol. 363, no. 13, pp. 1233–1244, 2010.

[10] E. M. van Rikxoort, B. de Hoop, S. van de Vorst, M. Prokop, and B. van Ginneken, "Automatic segmentation of pulmonary segments from volumetric chest CT scans." *IEEE Transactions on Medical Imaging*, vol. 28, no. 4, pp. 621–630, 2009.

[11] E. van Rikxoort, M. Prokop, B. de Hoop, M. Viergever, J. Pluim, and B. van Ginneken, "Automatic segmentation of pulmonary lobes robust against incomplete fissures," *IEEE Transactions on Medical Imaging*, vol. 29, no. 6, pp. 1286 –1296, 2010.

[12] J.-M. Kuhnigk, V. Dicken, S. Zidowitz, L. Bornemann, B. Kuemmerlen, S. Krass, H.-O. Peitgen, S. Yuval, H.-H. Jend, W. S. Rau, and T. Achenbach, "New tools for computer assistance in thoracic CT – part I: Functional analysis of lungs, lung lobes, and bronchopulmonary segments," *RadioGraphics*, vol. 25, no. 2, pp. 525–536, 2005.

[13] N. Sverzellati, E. Calabro, G. Randi, C. La Vecchia, A. Marchiano, J.-M. Kuhnigk, M. Zompatori, P. Spagnolo, and U. Pastorino, "Sex differences in emphysema phenotype in smokers without airflow obstruction," *European Respiratory Journal*, vol. 33, no. 6, pp. 1320–1328, 2009.

[14] S. Ukil and J. M. Reinhardt, "Anatomy-guided lung lobe segmentation in x-ray CT images." *IEEE Transactions on Medical Imaging*, vol. 28, no. 2, pp. 202–214, 2009.

[15] L. Zhang, E. A. Hoffman, and J. M. Reinhardt, "Atlas-driven lung lobe segmentation in volumetric X-ray CT images," *IEEE Transactions on Medical Imaging*, vol. 25, no. 1, pp. 1–16, 2006.

[16] J. Pu, B. Zheng, J. Leader, C. Fuhrman, F. Knollmann, A. Klym, and D. Gur, "Pulmonary lobe segmentation in CT examinations using implicit surface fitting," *IEEE Transactions on Medical Imaging*, vol. 28, no. 12, pp. 1986 –1996, 2009.

[17] K. Mori, Y. Nakada, T. Kitasaka, Y. Suenaga, H. Takabatake, M. Mori, and H. Natori, "Lung lobe and segmental lobe extraction from 3D chest CT datasets based on figure decomposition and voronoi division," in *Proceedings of SPIE Med Imaging*, vol. 6914, 2008.

[18] J. C. Ross, R. San Jose Estepar, A. Díaz, C.-F. Westin, R. Kikinis, E. K. Silverman, and G. R. Washko, "Lung extraction, lobe segmentation and hierarchical region assessment for quantitative analysis on high resolution computed tomography images," in *MICCAI*, ser. Lecture Notes in Computer Science, vol. 5762, 2009, pp. 690–698.

[19] J. C. Ross, R. San Jose Estepar, G. Kindlmann, A. Diaz, C.-F. Westin, E. K. Silverman, and G. R. Washko, "Automatic lung lobe segmentation using particles, thin plate splines, and maximum a posteriori estimation," in *MICCAI*, ser. Lecture Notes in Computer Science, vol. 6363, 2010, pp. 163–171.

[20] B. Lassen, J.-M. Kuhnigk, E. M. van Rikxoort, and H.-O. Peitgen, "Interactive lung lobe segmentation and correction in tomographic images," in *Proceedings of SPIE Med Imaging*, vol. 7963, 2011.

[21] B. Lassen, J.-M. Kuhnigk, O. Friman, S. Krass, and H.-O. Peitgen, "Automatic segmentation of lung lobes in CT images based on fissures, vessels, and bronchi," in *ISBI*, 2010, pp. 560–563.

[22] B. Lassen, J.-M. Kuhnigk, M. Schmidt, S. Krass, and H.-O. Peitgen, "Lung and lung lobe segmentation methods at Fraunhofer MEVIS," in *Proc. Fourth International MICCAI Workshop on Pulmonary Image Analysis*, Toronto, Canada, September 2011.

[23] J.-M. Kuhnigk, "Quantitative analysis of lung morphology and function in computed tomographic images," Ph.D. dissertation, 2008.

[24] B. van Ginneken, W. Baggerman, and E. M. van Rikxoort, "Robust segmentation and anatomical labeling of the airway tree from thoracic CT scans," in *MICCAI*, ser. Lecture Notes in Computer Science, vol. 5241, 2008, pp. 219–226.

[25] D. Selle, B. Preim, A. Schenk, and H.-O. Peitgen, "Analysis of vasculature for liver surgical planning," *IEEE Transactions on Medical Imaging*, vol. 21, no. 11, pp. 1344–1357, 2002.

[26] H. K. Hahn and H.-O. Peitgen, "IWT – interactive watershed transform: A hierarchical method for efficient interactive and automated segmentation of multidimensional gray-scale images," in *Proceedings of SPIE Med Imaging*, vol. 5032, 2003.

[27] E. van Rikxoort, J. Goldin, M. Galperin-Aizenberg, F. Abtin, H. Kim, P. Lu, B. van Ginneken, G. Shaw, and M. Brown, "A method for the automatic quantification of the completeness of pulmonary fissures: evaluation in a database of subjects with severe emphysema." *European Radiology*, vol. 22, pp. 302–309, 2012.

[28] F. Ritter, T. Boskamp, A. Homeyer, H. Laue, M. Schwier, F. Link, and H.-O. Peitgen, "Medical image analysis: A visual approach," *IEEE Pulse*, vol. 2, no. 6, pp. 60–70, 2011.

[29] MeVisLab, "Medical image processing and visualization (v2.3)," 2011, URL: www.mevislab.de.

[30] R. Beichel, M. de Bruijne, B. van Ginneken, S. Kabus, A. Kiraly, J.-M. Kuhnigk, J. McClelland, K. Mori, E. van Rikxoort, and S. Rit, Eds., *Proc. Fourth International MICCAI Workshop on Pulmonary Image Analysis*, Toronto, Canada, September 2011.